A&A 478, 513–520 (2008)
DOI: 10.1051/0004-6361:20077891
© ESO 2008

Astronomy & Astrophysics

XMM-Newton observations of ζ Orionis (O9.7 Ib): a collisional ionization equilibrium model⋆

A. J. J. Raassen[1,2], K. A. van der Hucht[1,2], N. A. Miller[3], and J. P. Cassinelli[4]

[1] SRON Netherlands Institute for Space Research, Sorbonnelaan 2, 3584 CA Utrecht, The Netherlands
e-mail: a.j.j.raassen@sron.nl
[2] Astronomical Institute "Anton Pannekoek", Kruislaan 403, 1098 SJ Amsterdam, The Netherlands
[3] Dept. of Physics & Astronomy, University of Wisconsin-Eau Claire, 105 Garfield Avenue, Eau Claire WI 54702, USA
[4] Dept. of Astronomy, University of Wisconsin at Madison, 6251 Sterling Hall, North Charter Str., Madison, WI 53706, USA

Received 15 May 2007 / Accepted 18 November 2007

ABSTRACT

We present *XMM-Newton* observations of the O supergiant ζ Orionis (O9.7 Ib). The spectra are rich in emission lines over a wide range of ionization stages. The RGS spectra show for the first time lines of low ion stages such as C VI, N VI, N VII, and O VII. The line profiles are symmetric and rather broad ($FWHM \approx 1500$ km s^{-1}) and show only a slight blue shift. With the XMM-EPIC spectrometer several high ions are detected in this star for the first time including Ar XVII and S XV.
Simultaneous multi-temperature fits and DEM-modeling were applied to the RGS and EPIC spectra to obtain emission measures, elemental abundances and plasma temperatures. The calculations show temperatures in the range ≈0.07–0.6 keV. According to the derived models the intrinsic source X-ray luminosity at a distance of 251 pc is $L_x = 1.37(.03) \times 10^{32}$ erg s^{-1} in the energy range 0.3–10 keV. In the best multi-temperature model fit, the abundances of C, N, O, and Fe are near their solar values, while the abundances of Ne, Mg, and Si appear somewhat enhanced.
The sensitivity of the He-like forbidden and intercombination lines to ζ Ori's strong radiation field is used to derive the radial distances at which lines are formed. Values of 34 R_* for N VI, 12.5 R_* for O VII, 4.8 R_* for Ne IX, and 3.9 R_* for Mg XI are obtained.

Key words. stars: early-type – stars: winds, outflows – X-rays: individual: ζ Orionis – X-rays: stars

1. Introduction

The object ζ Orionis is a supergiant of spectral type O9.7 Ib. Its X-ray spectrum has previously been observed with various satellites such as *Einstein* (Cassinelli & Swank 1983), *ROSAT* (Berghöfer et al. 1997), and *ASCA* (Kitamoto et al. 2000). The *Einstein* observations were particularly interesting: the Solid-State Spectrometer observations of ζ Ori were the first to show hot star X-ray emission lines, those of Si XIII and S XV (Cassinelli & Swank 1983).

From *ROSAT* observations Berghöfer et al. (1996) found that the X-ray emitting plasma could be characterized with an overall kT of 0.22 keV and that the X-ray to Bolometric luminosty ratio of $\log L_x/L_{bol} = -6.74$ is typical for O stars and early B supergiants. Based on *Chandra*-HETG data Waldron & Cassinelli (2001) concluded that most of the emission is at energies below 1 keV.

It is generally believed that most of these X-rays received from O stars originate in shocks distributed throughout the wind, and that these shocks are created by instabilities in the line-driving mechanism which drives the overall outflow (e.g., Lucy & Solomon 1970; Lucy 1982; Owocki et al. 1988; Dessart & Owocki 2005). To explore the relation between the X-ray emission from ζ Ori and the properties of the shocks in its wind line profiles from high-resolution *Chandra* observations were used by Cohen et al. (2006), Owocki & Cohen (2006), and Oskinova et al. (2006).

Waldron & Cassinelli (2001) also analyzed the ratios of the forbidden (f), the intercombination (i) and the resonance (r) emission lines in the He-like ions of Si XIII, Mg XI, Ne IX, and O VII. The lines were found to be produced at a wide range of radii. The specific radius for each He-like ion was found to correspond to X-ray optical depth unity to the continuum opacity at each line wavelength. Their most surprising result was that the high ion stages, such as Si XIII, appear to form very close to the star. At these close distances the shock velocity jump was found to be larger than could be explained by the speed that the wind should have at these small radii.

Recently Pollock (2007a) developed a new paradigm for O-star X-ray emission, which states that charge exchange, ionization, and excitation are likely to be produced by protons far out in the wind. However, this approach is not yet capable of describing the spectrum and line fluxes in a quantitative way, and so it will not be discussed further in this paper.

Variability has been found in both ζ Ori's Hα profile (Ebbets 1982; Kaper et al. 1997) and its UV P-Cygni profiles (Snow 1977; Kaper et al. 1996, 1999). However, the X-ray light curve has provided no evidence for variability over a long time range (Berghöfer & Schmitt 1994).

In many of the recent papers the authors have focussed on line profiles and individual line features. This is especially true for spectra obtained by means of the high resolution instruments aboard *Chandra* (HETG and MEG). In contrast RGS aboard

⋆ Appendix A is only available in electronic form at http://www.aanda.org

Article published by EDP Sciences and available at http://www.aanda.org or http://dx.doi.org/10.1051/0004-6361:20077891

Table 1. Observation log of the data of ζ Ori.

Instr.	Filter	Mode	Date-obs-start	Date-obs-end	Duration (s)
MOS1	Thick	Small Window	2002-09-15T13:12:32	2002-09-16T00:51:00	41 728
MOS2	Thick	Timing	2002-09-15T13:12:28	2002-09-16T00:46:41	41 473
pn	Thick	Full Frame	2002-09-15T14:04:08	2002-09-16T00:51:20	38 362
RGS1	None	Spec+Q	2002-09-15T13:11:17	2002-09-16T00:52:38	41 979
RGS2	None	Spec+Q	2002-09-15T13:11:17	2002-09-16T00:52:38	41 979

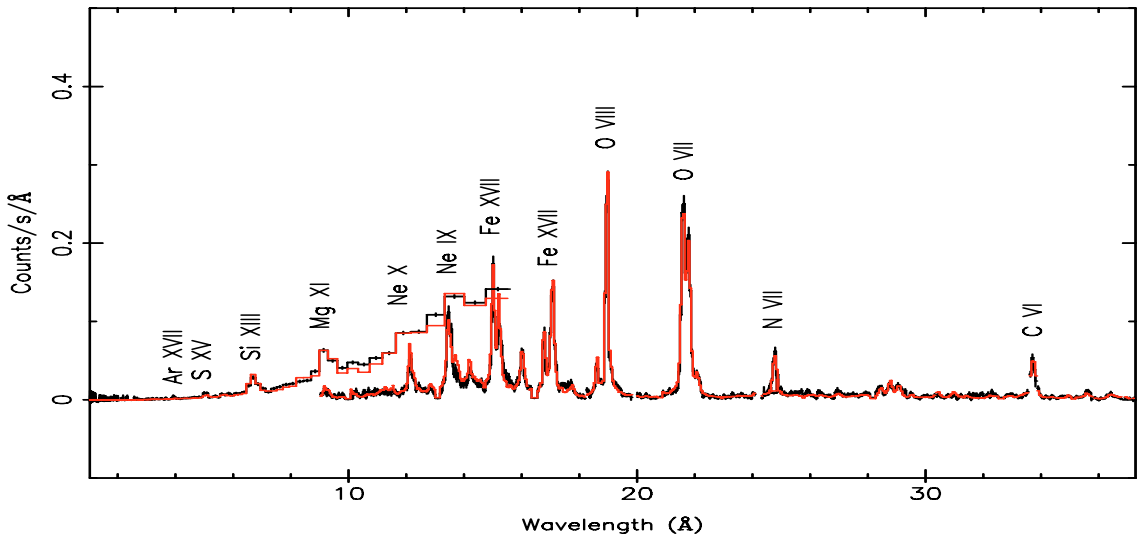

Fig. 1. Background-subtracted EPIC-MOS and first-order RGS spectra of ζ Ori. Error bars indicate 1σ statistical errors including the effect of background. The grey (red in the electronic version) curve shows the best-fit model. A number of prominent lines are labeled with the emitting ions.

XMM-Newton provides us with new information regarding the longer wavelength part of the spectrum where ion stages such as C VI, N VI, and N VII can be observed. In addition, the higher collecting area of *XMM-Newton* allows us to obtain a better estimate of the distribution of emission measure versus temperature. In the present paper the spectra and line-fluxes of ζ Ori, observed with *XMM*-EPIC and -RGS, are described for the first time by means of a multi-temperature fit and DEM-modeling to the total spectrum. The approach we choose to take is to use emissivity results from optically thin Coronal Ionization Equilibrium (CIE) plasma calculations.

Apart from this broad description of the total spectrum, individual line fluxes and line ratios are analyzed in this paper. Ratios of the *fir* lines of He-like ions are used to determine the typical distances between the X-ray emission regions and the stellar photosphere. The wavelength sensitivity of *XMM-Newton* allows us to check the results of Waldron & Cassinelli (2001) for Mg XI, Ne IX, and O VII (with somewhat more precise radial ranges), while extending the analysis to include the N VI lines. The results for the lines of N VI are particularly interesting because this is the first time that this line ratio has been interpreted in this manner for this star.

ζ Ori was observed on 2002 September 9 by means of *XMM-Newton*. A log of these observations is shown in Table 1. The spectral analysis by means of multi-temperature fitting and DEM-modeling are described in Sect. 2. The analysis of the line profiles and the individual line fluxes, including several that have not been studied earlier, is given in Sect. 3. The results are discussed in Sect. 4. Parameters of ζ Ori are given in Table A.1 in the appendix.

2. Spectral analysis

2.1. Multi-temperature fitting

We have determined the thermal structure and the elemental composition of ζ Ori's X-ray emitting plasma by simultaneously fitting multi-temperature models to the RGS, EPIC-MOS1, and PN spectra. The fit was performed using our spectral analysis program SPEX (Kaastra et al. 1996a) in combination with the MEKAL (Mewe-Kaastra-Liedahl) code, as developed by Mewe et al. (1985, 1995) (see Fig. 1). MEKAL calculates a continuum and models more than 5400 spectral lines. It is available on the WWW[1]. The applied model is a Collisional Ionization Equilibrium (CIE) model for optically thin plasma. The ionization equilibrium is based on calculations by Arnaud & Rothenflug (1992) and Arnaud & Raymond (1985).

2.1.1. Temperature and emission measure

In the multi-temperature calculations we used initially five temperatures. Out of the five fitted temperature components three turn out to be significant. These three temperature components were coupled to one $N_{\rm H}$ absorption column density and one set of abundances, which were free to vary. The column density, temperatures, emission measures $EM = \int n_{\rm e} n_{\rm H} {\rm d}V$, X-ray luminosities, elemental abundances, and micro-turbulent velocity ($v_{\rm mic}$) are given in Table 2, together with the statistical 1σ uncertainties. Three temperatures at $T = 0.073$ keV, $T = 0.201$ keV and $T = 0.551$ keV were determined. Interpreting the results in terms of a wind with embedded shocks and using

[1] http://www.sron.nl/divisions/hea/spex/

Table 2. Multi-temperature fitting for combined EPIC-PN, EPIC-MOS1 & RGS spectra of ζ Ori[a].

Comp. i	Value	
N_H[b]	5.0	
kT_1[c]	0.551 ± 0.013	
EM_1[d]	1.57 ± 0.18	
L_{x1}[e]	4.18	
L_{x1}[f]	3.8	
v_{mic1}[g]	1080 ± 135	
kT_2[c]	0.201 ± 0.004	
EM_2[d]	3.76 ± 0.31	
L_{x2}[e]	6.71	
L_{x2}[f]	20.6	
v_{mic2}[g]	950 ± 70	
kT_3[c]	0.073 ± 0.006	
EM_3[d]	10.1 ± 2.7	
L_{x3}[e]	2.8	
L_{x3}[f]	111.0	
v_{mic3}[g]	1240 ± 230	
$\sum_i EM_i$[d]	15.4 ± 2.2	
$\sum_i L_{xi}$[e]	13.7 ± 0.3	
$\sum_i L_{xi}$[f]	135 ± 4	
z_{red}[h]	-3×10^{-4}	
	Abundance[i]	
	A_i	A_i/A_O
C	1.02 ± 0.11	1.20 ± 0.05
N	1.03 ± 0.09	1.21 ± 0.05
O	0.85 ± 0.07	1
Ne	1.33 ± 0.15	1.57 ± 0.07
Mg	1.66 ± 0.16	1.96 ± 0.08
Si	1.30 ± 0.14	1.54 ± 0.05
Fe	0.99 ± 0.09	1.15 ± 0.06
χ^2_{red}	1246/1064 = 1.17	

Notes:
[a] *HIPPARCOS* distance $d = 0.25$ kpc is used.
[b] Column density (10^{20} cm^{-2}) derived for standard absorption model (with solar abundances) from Morrison & McCammon (1983) for all components.
[c] Temperature in keV.
[d] Emission measure in 10^{54} cm^{-3}.
[e] X-ray luminosity of the instrumental *XMM-Newton* band (0.3−10 keV) in 10^{31} erg s^{-1}.
[f] X-ray luminosity of the total emission range, 0.03−0.9 keV (see Fig. 2), in 10^{31} erg s^{-1}.
[g] Micro-turbulent velocity parameter used to characterize line broadening (in km s^{-1}).
[h] Artificial redshift to match the observed wavelengths to the theoretical ones.
[i] Abundance relative to solar photospheric number abundance (Anders & Grevesse 1989 for all ions except Fe, where Grevesse & Sauval 1998, 1999 was used).

$kT = 1.2\ [v(1000\ \mathrm{km\ s^{-1}})]^2$ keV, we find that the kT range from 0.073 keV to 0.551 keV corresponds to shock jumps from 246 km s^{-1} to 676 km s^{-1}. These are well below the terminal wind speed of 1885 km s^{-1} (=2.3 keV), so they seem physically reasonable.

Out of the three EM values the most uncertain is the one corresponding to the lowest temperature component (T = 0.07 keV). This component is determined by the C VI and N VI features. The most robust of the three components is the one at 0.20 keV because it involves the largest number of emission lines in the spectrum. The EM values for ζ Ori decrease with T and approximately follow the relation $EM \propto T^{-0.8}$.

The total EM over the three temperature bins is 1.35×10^{55} cm^{-3}. It is interesting to compare these values to the "wind emission measure" EM_w given by Cassinelli et al. (1981). Based on their formula we obtain for ζ Ori $EM_w = 2.44 \times 10^{58}$ cm^{-3}. This shows that only a small fraction of the wind is contributing to the X-ray spectrum.

The emission lines observed in ζ Ori's X-ray spectrum clearly exhibit Doppler broadening of roughly 1000 ± 100 km s^{-1}. Therefore, the lines generated in the model spectrum need to be broadened in excess of instrumental effects to allow a reasonable comparison with the data. For this purpose, we used the micro-turbulent velocity parameter (v_{mic}) available in SPEX. In using this parameter, we do not mean to imply that the emission line broadening is microturbulent in nature, rather, it is just a convenient way to parameterize the line broadening due to the outflow of the X-ray emitting regions. The v_{mic} parameter is related to the $FWHM$ measure of the line broadening through the relation $FWHM/E_{obs} = 2\sqrt{\ln 2}\, v_{mic}/c$. Here E_{obs} is the energy of the emission line, i.e. $12.39842/\lambda_{obs}$. A characteristic value used in the fitting was $FWHM/E_{obs} = 5.5 \pm 0.5 \times 10^{-3}$.

To achieve the best fit possible, the overall Doppler shift parameter z_{red} was used. The best fits were achieved using an overall blueshift of roughly 100 km s^{-1}. To interpret this number, it is interesting to note that some small blueshift of the spectral line centroids is to be expected due to the attenuation of the X-rays emitted from shocks moving away from the observer on the far side of the wind. Nonetheless, the fact that this shift is roughly of the order of systematic uncertainties in the wavelength calibration (Pollock 2007b) means this result should be viewed with some caution. The interpretation of individual emission line shapes is considered in more detail in Sect. 3.

2.1.2. Abundances

The elemental abundances are relative to solar photospheric values from optical studies (Anders & Grevesse 1989) except for Fe, for which we use $\log A_{Fe} = 7.50$[2] (see Grevesse & Sauval 1998, 1999) instead of 7.67 (Anders & Grevesse 1989).

The abundances have been determined through a fit to the total spectrum, allowing them to freely vary along with the emission measures and temperatures. When interpreting these abundance measurements, two issues should be kept in consideration: first, the abundances are strongly anti-correlated with the emission measures (especially in cases involving a weak continuum), with the result that the products of emission measure and abundance ($EM \times A_i$) are quite robust. Second, the ratios between the abundances (A_i/A_O or A_i/A_{Fe}) of the various elements are more robust than the absolute abundances themselves. Therefore, the ratios between the abundances are often presented in papers. Here we give both values, the absolute abundances and the ratio of the elemental abundance over the oxygen abundance averaged for a number of fits.

The carbon abundance is strongly related to the lowest temperature and the corresponding emission measure. Almost 50% of the line flux of this ion is produced by the lowest temperature component. The obtained abundances are all close to solar photospheric values except for Ne, Mg, and Si. This behaviour is different from coronal plasmas, for which in the quiescent state a First Ionization Potential (FIP) effect is noticed. This effect

[2] Here $\log A_{Fe}$ is the logarithm of the Fe-abundance relative to $\log A_H = 12.0$.

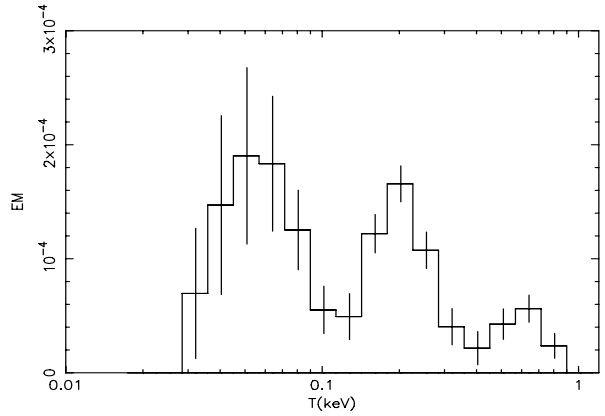

Fig. 2. DEM modeling of the EPIC-MOS and RGS spectra of ζ Ori. The emission measure EM per logarithmic temperature bin is in units of 10^{58} cm^{-3}.

implies that elements with low first ionization potential (Mg, Si, Fe) are overabundant in the corona compared to the photosphere. For active, flaring coronal plasma an inverse FIP effect is often found.

2.1.3. X-ray luminosity

The luminosity is a robust quantity. The X-ray luminosities, given in Table 2, are the model luminosity in the band 0.3−10 keV (the energy range of *XMM-Newton*) and in the energy band 0.03−0.9 keV, the energy range of the determined emission measure (see Fig. 2). Both values correspond to the location of the emitting plasma, i.e., they are corrected for absorption by the interstellar medium (ISM) and by the stellar wind. Our instrumental (0.3−10 keV) value of $L_{\rm x} = 1.37 \times 10^{32}$ erg s^{-1} results in a value for $\log L_{\rm x}/L_{\rm bol} = -6.66(.09)$ which is similar to the values obtained using *Einstein* (Chlebowski et al. 1989) and *ROSAT* (Berghöfer et al. 1996).

In order to attribute the X-ray emission from this star to shocks embedded in its wind, some of the mechanical energy of the wind outflow must be converted into heat energy. It is therefore interesting to compare the measured X-ray luminosity to the mechanical luminosity of the wind, a quantity which can easily be calculated from a formula given in Howk et al. (2000). The resulting value of $L_{\rm w} = 1.6 \times 10^{36}$ erg s^{-1} should be compared with the X-ray luminosity of the total emission of $L_{\rm x} = 1.4 \times 10^{33}$ erg s^{-1}. This indicates that only about a one thousandth of the mechanical energy available in the wind is radiated away as X-rays, a small fraction.

2.2. DEM modeling

Apart from a multi-T fitting, the combined EPIC-MOS, EPIC-PN, and RGS spectrum was also fitted by means of a differential emission measure (DEM) modeling (e.g., Kaastra et al. 1996b) using the regularization module in SPEX. This module constructs an emission measure distribution with the constraint that the first and second derivatives are smooth and continuous. We define the DEM by $n_{\rm e} n_{\rm H} {\rm d}V/{\rm dlog}\,T$ (integrated over one logarithmic temperature bin, the emission measure = $n_{\rm e} n_{\rm H} V$).

The result for the emission measure distribution EM is shown in Fig. 2. The temperature covers the range from 0.03 keV to 0.9 keV, i.e., from 0.3 to 10 MK, with three temperature peaks around 0.06 keV, 0.2 keV, and 0.6 keV. These values are consistent with the results of the 3-T fittings. Just as in the case of the 3-T fitting the DEM-modeling is most robust for the range around 0.2 keV, while the error bars are larger for the low temperature regime.

3. Emission line fluxes

As mentioned in the introduction, the shapes of the X-ray emission lines detected by high resolution X-ray spectrometers have been very important in determining the nature of the X-ray emission from these stars. Therefore, apart from the description of the total X-ray spectrum of ζ Ori by means of a CIE model, the fluxes, wavelengths, and broadenings of the individual emission lines were measured. This was done by folding a Gaussian through the response matrix.

In cases where line blending would interfere with a measurement, we adopted the following procedure to isolate the contribution of the line being measured: The parameters derived in the multi-T fit (Sect. 2.1.1.) were used to generate a model spectrum which included the contributions of all relevant ions *except* the ionization state of the line being measured. A single Gaussian (whose parameters were free to vary in the fit) was then added on top of the computed model spectrum to measure the individual contribution of the line being measured.

In Table 3 the wavelengths, the measured fluxes at Earth (not corrected for interstellar absorption), and the widths of a number of prominent lines are collected. Within brackets the 1σ errors are given. The rest wavelengths (λ_0) are taken from Kelly (1987) and Dere et al. (2001),

3.1. Analysis of emission line profiles

The lines in the RGS spectrum of ζ Ori are symmetric, broadened and slightly blue-shifted. After correcting for instrumental broadening, $FWHM$ is ≈1500 km s^{-1} (cf. Table 3). For the dominant, unblended lines of C VI (33.736 Å), N VII (24.781 Å), O VIII (18.969 Å), Fe XVII (15.013 Å), and Ne X (12.134 Å) we obtain a $FWHM$ of 1540(240) km s^{-1}, 1500(360) km s^{-1}, 1600(140) km s^{-1}, 1440(260) km s^{-1}, and 1400(600) km s^{-1}, respectively. Our results confirm the observations done with the *Chandra*-HETGS (Waldron & Cassinelli 2001; Miller 2002; Miller et al. 2002). The line broadenings of the individual line measurements are consistent with the relative broadening $FWHM/E_{\rm obs}$ of 5.5 (in units 0.001), determined by means of the $v_{\rm mic}$ value of the multi-temperature fit in Sect. 2.1.1. For the same lines as mentioned above the values of $FWHM/E_{\rm obs}$ are 5.2(0.8), 5.0(1.2), 5.4(0.5), 4.8(0.8), and 4.7(1.9), respectively. This broadening is consistent with a picture of outwardly moving shocks.

Most wavelengths of the lines in Table 3 show a negative deviation, corresponding to ≈−90(60) km s^{-1}, which is based on the same five lines as used above with individual deviations of −200(90) km s^{-1}, −120(110) km s^{-1}, −75(50) km s^{-1}, −20(80) km s^{-1}, and −70(200) km s^{-1}. There is some tendency that the features of the lower ionized (cooler) ions are more blue-shifted. However, due to the large errors, the evidence for blue-shifted line profiles is not very strong.

The possible effects of resonance line scattering opacity on the shapes of hot star X-ray emission lines have been discussed in Leutenegger et al. (2007) and Ignace & Gayley (2002). We use the measured line fluxes of Fe XVII to estimate the optical thickness of the shock sources of ζ Ori. In an optically thin plasma, the line flux ratio of the Fe XVII lines at 15.013 Å and 15.260 Å would be expected to be 3.5(1.0) from the MEKAL atomic data,

Table 3. Measured line fluxes at Earth of ζ Orionis. Statistical 1σ errors in the last digits in parentheses.

ion	λ_0^a [Å]	$\lambda_{\rm obs}^a$ [Å]	$\Delta\lambda^b$ [Å]	Δv^c [km s^{-1}]	flux [10^{-13} erg cm^{-2} s^{-1}]	*FWHM*^{d} [10^{-3} keV]	*HWHM*^{e} [km s^{-1}]
EPIC							
Ar XVII	3.949	3.92(.031)	–	–	0.07(.03)	–	–
S XV	5.039	5.032(.018)	–	–	0.18(.05)	–	–
Si XIII	6.692	6.684	–	–	0.84(.42)	–	–
Mg XI	9.170	9.177(.014)	–	–	1.18(.09)	–	–
RGS							
Si XIII	6.692	6.688(.066)	–	–	0.84(.60)	–	–
Mg XII	8.423	8.405(.030)	–	–	0.27(.13)	–	–
Mg XI	9.169	9.169^f	–	–	0.59(.15)	7.5(7.5)	800(800)
Mg XI	9.231	9.231^f	–	–	0.31(.14)	7.5(7.5)	800(800)
Mg XI	9.313	9.313^f	–	–	0.33(.12)	7.5(7.5)	800(800)
Ne X	10.240	10.212(.020)	–.028	–820(590)	0.29(.14)	<11.0	<1330
Ne X	12.134	12.131(.008)	–.003	–70(200)	1.83(.26)	4.8(1.9)	700(300)
Fe XVII	12.264	12.256(.023)	–.008	–200(600)	0.61(.19)	4.8(1.9)	700(300)
Ne IX	13.447	13.444(.006)	–.003	–70(130)	3.35(.39)	3.8(1.0)	620(160)
Ne IX	13.553	13.548(.009)	–.005	–110(200)	2.26(.32)	3.8(1.0)	620(160)
Ne IX	13.700	13.699(.017)	–.001	–20(400)	0.66(.20)	3.8(1.0)	630(170)
Fe XVIII	14.205	14.204(.011)	–.001	–20(220)	0.79(.18)	3.7(3.0)	640(515)
Fe XVII	15.013	15.012(.004)	–.001	–20(80)	5.33(.33)	4.0(0.7)	720(130)
O VIII	15.176	15.176^f	–	–	0.99(.44)	4.0(0.7)	720(130)
Fe XVII	15.260	15.261(.014)	+.001	+20(280)	2.16(.42)	4.0(0.7)	720(130)
Fe XVII	15.449	15.415(.026)	–.034	–700(500)	0.54(.26)	<8.3	<1550
O VIII	16.006	16.017(.008)	+.011	+210(150)^h	2.21(.29)	4.9(1.2)	950(230)
Fe XVIII	16.078	–	–	–	–	–	–
Fe XVII	16.775	16.771(.006)	–.004	–70(110)	2.04(.22)	2.0(1.1)	410(220)
Fe XVII	17.051	17.051^i	–	–	2.84(.52)	3.7(0.9)	760(190)
Fe XVII	17.100	17.100^i	–	–	2.34(.42)	4.7(1.3)	970(270)
O VII	17.396	17.386(.034)	–.010	–170(600)	0.62(.23)	–	–
O VII	17.768	17.740(.014)	–.028	–500(250)	0.64(.12)	4.0(1.5)	860(320)
O VII	18.627	18.617(.009)	–.010	–160(144)	1.10(.16)	3.9(0.8)	880(180)
O VIII	18.969	18.962(.003)	–.007	–75(50)	10.78(.36)	3.5(0.3)	800(70)
O VII	21.602	21.594(.005)	–.008	–110(70)	8.07(.60)	2.4(0.3)	630(80)
O VII	21.804	21.775(.007)	–.029	–400(100)	8.44(.63)	3.8(0.4)	1000(110)
O VII	22.101	22.088(.009)	–.013	–180(120)	0.93(.15)	3.0(0.7)	800(190)
N VII	24.781	24.771(.009)	–.010	–120(110)	1.44(.14)	2.5(0.6)	750(180)
N VI	24.898	24.898(.041)	–.000	0(490)	0.34(.16)	1.8(0.6)	530(180)
Ca XIII	26.719	26.712(.055)	–.007	–80(640)	0.13(.08)	<2.4	<790
C VI	26.990	26.972(.024)	–.018	–200(270)	0.24(.09)	<2.2	<720
Ar XIV?	27.41	27.343(.029)	–.067	–700(320)	0.19(.10)	<5.0	<1600
Ca XII	27.973	27.955(.027)	–.018	–190(300)	0.25(.10)	1.6(1.3)	540(440)
C VI	28.466	28.396(.031)	–.070	–700(300)	0.62(.12)	2.9(1.5)	1000(520)
N VI	28.787	28.771(.027)	–.016	–170(280)	0.79(.12)	3.0(0.6)	1040(210)
N VI	29.084	29.076(.027)	–.009	–90(280)	0.97(.14)	3.0(0.6)	1050(210)
N VI	29.534	29.521(.059)	–.013	–130(600)	0.21(.07)	3.0(0.6)	1070(210)
S XIV	30.441	30.427(.023)	–.014	–140(230)	0.16(.08)	<1.0	<370
Si XII	31.016	30.959(.033)	–.057	–550(320)	0.17(.07)	<2.4	<900
S XIII	32.22	32.226(.030)	–	–	0.22(.08)	<1.7	<660
S XIV	32.554	32.527(.043)	–.027	–250(400)	0.28(.09)	<2.2	<870
C VI	33.736	33.713(.010)	–.023	–200(90)	2.96(.33)	1.9(0.3)	770(120)
S XIII	35.66	35.622(.021)	–	–	0.53(.08)	1.5(0.5)	650(220)
S XII	36.398	36.350(.030)	–.048	–400(250)	0.40(.10)	1.3(0.7)	570(310)

Notes:
^{a} λ_0 is theoretical wavelength from Kelly (1987) and Dere et al. (2001) and $\lambda_{\rm obs}$ is observed wavelength with the statistical 1σ error in parentheses; ^{b} line wavelength shift; ^{c} velocity shift; ^{d} line broadening *FWHM*; ^{e} line half-width at half maximum; ^{f} line wavelength fixed to assumed "blue-shifted" value; ^{h} if we take the average wavelength for the O VIII, Fe XVIII blend then we obtain a velocity shift of –500 km s^{-1}; ^{i} line wavelength fixed to theoretical value.

while the measured ratio for our ζ Ori data is 2.5(0.5). Thus we can conclude that there is no severe resonance line scattering in the Fe XVII line at 15.013 Å and that the individual line source regions are optically thin, even though the entire wind is thick to X-rays at these wavelengths.

The measured line fluxes of the He-like lines of N VI, O VII, Ne IX, and Mg XI are used in the next section.

It is likely the weak features in the EPIC-MOS spectrum near 3.9 Å and 5.0 Å are due to Ar XVII and S XV, respectively. The optimal formation temperatures of these ions (22 MK or

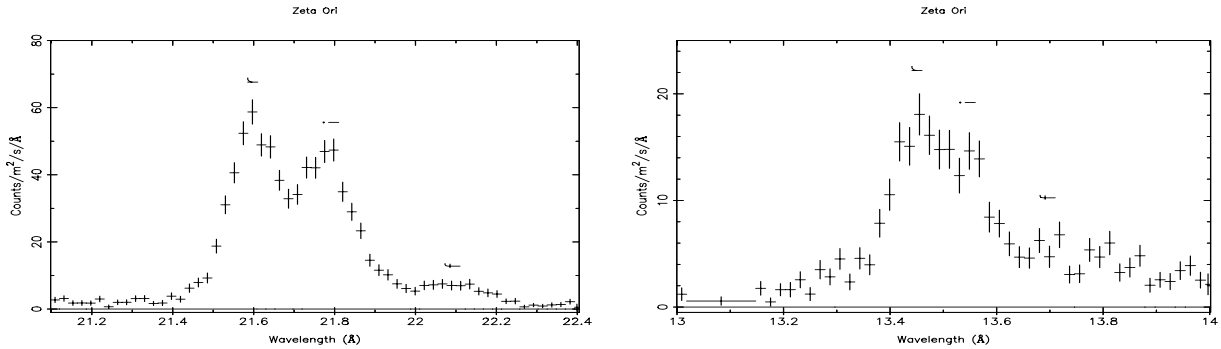

Fig. 3. The panels show the He-like O VII and Ne IX line triplets consisting of a resonance line (r), an intercombination line (i), and a forbidden line (f) for the O9.5Ib star ζ Ori. In both panels, the forbidden line nearly disappears due to radiative depopulation of the upper level in the strong radiation field relatively close to the surface of the star.

1.9 keV, and 16 MK or 1.4 keV, respectively) are much higher than any of the temperatures found in our three-temperature and DEM temperature modeling in Sect. 2. The presence of emission lines from these ions indicates that they are formed in a high energy tail in the emission measure distribution of this star and in the wings of the line profiles.

3.2. He-like line diagnostics

Gabriel & Jordan (1969) were the first to demonstrate that forbidden (f), intercombination (i) and resonance (r) lines of the He-like "complexes" provide useful diagnostics for X-ray emitting plasmas. The most recent studies including the effects of dielectronic satellite lines and a radiation field have been done by Porquet et al. (2001). The ratio f/i is dependent on electron density because of the depopulation of the upper level of the f line in favour of the upper level of the i line at increasing density. This effect can be used to derive electron densities in circumstances where radiation fields are relatively weak, such as in cool stars. However, in OB stars, where the radiation fields are much stronger, the depopulation of the upper level of the f line in favour of the upper level of the i line occurs by radiative absorption (e.g., Blumenthal et al. 1972; Porquet et al. 2001). The f/i ratio no longer indicates the density, but instead provides information on the mean intensity of the radiation field, hence the radial distance R of the X-ray source from the star. This is illustrated in Fig. 3 for the Ne IX and O VII triplets. It is seen that the forbidden line is nearly suppressed for both ions.

The fact that the UV radiation field is the dominant effect for ζ Ori is confirmed by detailed calculations. Using the formalism developed by Blumenthal et al. (1972), we calculate the radial dependence of R in the envelope of ζ Ori on the basis of a Planck curve (Ness et al. 2001) of 31 500 K as well as on the basis of a photospheric model of Vacca et al. (1996) with $T_{\rm eff}$ = 32 000 K and $\log g$ = 3.23 and applying a UV flux model OSTAR2002 of Lanz & Hubeny (2003) with $T_{\rm eff}$ = 32 500 K, $\log g$ = 3.25, and solar metallicity. These parameters closely correspond to those given in the appendix. The radial-dependent wind density is derived from the stellar and wind parameters of Lamers & Leitherer (1993) using a standard velocity law that is modified below 1.02 R_* (where R_* is the stellar radius) to provide a smooth density transition to the photospheric structure. The mean intensity of the UV radiation is large near the surface of the star and it decreases outwards by dilution factor $W(r) = \frac{1}{2}\left[1-\left(1-\left(\frac{R_*}{r}\right)^2\right)^{1/2}\right]$. As a result of the radial dependence of the radiation field, the observed f/i ratio can be

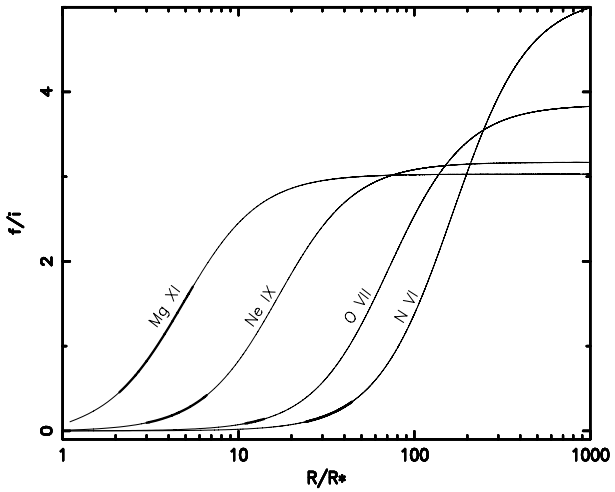

Fig. 4. The curves show the expected f/i line ratio as a function of formation radius R for the labeled He-like ions. The thickened portion of each line gives the radial range of the X-ray emission implied by the measured f/i line ratios.

used to derive the radial location of the He-like ions that are producing the observed fir lines. For the four He-like ions which allow reliable measurements of their f/i line ratio (N VI, O VII, Ne IX, and Mg XI) these parameters indicate that ζ Ori's radiation field will suppress the forbidden lines by radiative de-excitation of the upper level of f to much greater radii than would be possible with collisions (see, e.g., Waldron & Cassinelli 2001). Thus the expected f/i ratios as functions of radii for these ions are entirely controlled by the strength of ζ Ori's UV radiation field.

The predicted R dependencies of f/i are shown in Fig. 4. The f/i ratios derived from the RGS spectra for N VI, O VII, Ne IX, and Mg XI are: 0.22 ± 0.12, 0.114 ± 0.027, 0.26 ± 0.16, and 1.08 ± 0.61, respectively (cf. Table 3), agreeing with values for Ne IX and Mg XI given by Oskinova et al. (2006). These ratios correspond to average distances from the stellar surface R of the ion formation of 34 ± 10 R_*, 12.5 ± 1.5 R_*, 4.8 ± 1.8 R_*, and 3.9 ± 1.7 R_*, respectively. For the last three ions this is in agreement with values established by Waldron & Cassinelli (2001), based on HETGS observations. They determined values for formation radii of $\lesssim$12 R_* for O VII, of $\lesssim$6 R_* for Ne IX, and 3−5 R_* for Mg XI.

The formation distances of He-like ions increase with decreasing ionization stage, but they increase also with increasing

wavelength (λ) of the line triplets. The formation distance is proportional to some power of the wavelength of the intercombination line (λ^p, with $p \approx 2.5$–4.5). Waldron & Cassinelli (2001) pointed out that the derived radii ($R_{\rm fir}$), at which the He-like lines are observed, are strongly correlated with the radii R_λ at which the continuum adjacent to the line has an optical depth unity. Since the opacity varies roughly as λ^3 this correlation would mean that we are observing the He-like lines from the deepest possible part of the wind from which X-rays could escape to the observer.

Leutenegger et al. (2006) give estimates for minimum radii of formation of the hot plasma for O-stars. Their values for minimum radii are about 1.5 R_*, based on the ions of higher stages of ionization (S XV, Si XIII, and Mg XI). The reader should keep in mind that our measurements of the radii of line formation are not directly comparable to theirs. Our values are average values with a lower and higher limit due to the uncertainty in the measured line fluxes and do not imply a minimum or maximum distance of ion formation.

Finally, we used the resonance line, the forbidden line, and the intercombination line of the He-like lines as a temperature diagnostic for the individual regions responsible for the fir emission of each ion. As a single-temperature measurement method for specific regions in the wind, this method gives independent, complementary information to the global temperature fitting carried out in Sect. 2. Using the results of Porquet et al. (2001) we extract from the measured $(i + f)/r$ ratios (cf. Table 3) for N VI, O VII, and Ne IX electron temperatures of about 0.05, 0.16, and 0.24 keV, respectively. These three temperatures are in the range of the lower two of the three temperatures found with multi-temperature fitting in Sect. 2.1.1.

4. Discussion of results and conclusion

The O supergiant ζ Orionis (O9.7 Ib) has a line rich X-ray spectrum. The spectral lines are symmetric and broadened. The *FWHM* corresponds to 1500 km s^{-1}; less than the terminal speed of 1885 km s^{-1} derived by Lamers et al. (1999). The velocity widths are consistent with a picture of outwardly propagating shocks that are distributed throughout the wind and that are produced by the instabilities associated with a line-driven wind. The best fits require a small blue-shift. It should be noted, however, that this blue-shift is of the order of the calibration uncertainties of the instrument.

The continuum and line features are very well described by a 3-T collisional ionization equilibrium model (CIE) for optically thin plasma, using SPEX in combination with MEKAL. The determined temperatures range from 0.07 to 0.55 keV (0.85–6.4 MK), corresponding to shock jumps from 246 km s^{-1} to 676 km s^{-1}. The total X-ray luminosity of the star corresponds to an emission measure that is far below the emission measure of the entire wind (Cassinelli et al. 1981; Cassinelli & Swank 1983), indicating that only a small fraction of the wind is participating in the X-ray emission.

We used the values of the forbidden to intercombination line ratio of He-like ions to derive characteristic radii of line formation. For Mg XI, Ne IX, O VII, and N VI, this resulted in values of 4, 5, 12.5, and 34 stellar radii, respectively.

The hotter and higher ionized ions are on average formed deeper in the wind, closer to the stellar surface. This is in agreement with values established by Waldron & Cassinelli (2001), based on HETGS observations. Applying the standard beta velocity law $v(r) = v_\infty \left(1 - \frac{R_*}{r}\right)^\beta$, with $\beta = 0.7(.1)$ (Groenewegen & Lamers 1989) we obtain at a distance of 4 R_* (where the hotter plasma of Mg XI is located) $v(r) = 0.82 \times v_\infty = 1540$ km s^{-1}. This velocity is far higher than the velocity jump necessary to produce the high temperatures.

Waldron & Cassinelli (2001) found that line diagnostics for Si XIII indicate that this line emission forms very close to the stellar surface, where the velocity is too small to produce the shock jump required for the observed ionization level. The analysis of 17 O stars by Waldron & Cassinelli (2007) has led to a strengthening of this conclusion. However, due to the lower resolution of the RGS relative to that of the HETGS on *Chandra* and the weakness of the relevant lines in our spectrum, we cannot investigate the formation radius of Si XIII. These limitations therefore preclude us from confirming or denying the presence of this effect in the X-ray emission of ζ Ori.

We conclude that our results are consistent with a model of shock fragments that are embedded in the wind and are expanding outward with the wind. The Fe XVII line ratios indicate that the individual source regions associated with the shock fragments are optically thin. The lack of variability of the X-rays over the years implies a large number of sources embedded in the wind. Ions are found to be formed and emitting both from far out and deep in the wind. The symmetry of the line profiles and the slight blue-shift are consistent with the "porosity model" (Feldmeier et al. 2003; Oskinova et al. 2006; Owocki & Cohen 2006, and Fig. 4 therein), though we find a wider range in line formation radii than the $\approx$1.5 R_* used in their scenario.

Acknowledgements. This work is based on observations obtained with *XMM-Newton*, an ESA science mission with instruments and contributions directly funded by ESA Member States and the USA (NASA). The SRON Netherlands Institute for Space Research is supported financially by NWO. J.P.C. and N.A.M. acknowledge support from NASA grants NAG5 5-9226 and GO2-3028, respectively.

References

Anders, E., & Grevesse, N. 1989, Geochim. Cosmochim. Acta, 53, 197
Arnaud, M., & Raymond, R. 1992, ApJ, 398, 394
Arnaud, M., & Rothenflug, J. 1985, A&AS, 60, 425
Berghöfer, T. W., & Schmitt, J. H. M. M. 1994, A&A, 290, 435
Berghöfer, T. W., Schmitt, J. H. M. M., & Cassinelli, J. P. 1996, A&AS, 118, 481
Berghöfer, T. W., Schmitt, J. H. M. M., Danner, R., & Cassinelli, J. P. 1997, A&A (Letters), 322, 167
Blumenthal, G. R., Drake, G. W. F., & Tucker, W. H. 1972, ApJ, 172, 205
Cassinelli, J. P., & Swank, J. H. 1983, ApJ, 271, 681
Cassinelli, J. P., Waldron, W. L., Sanders, W. T., et al. 1981, ApJ, 250, 677
Cassinelli, J. P., Miller, N. A., Waldron, W. L., MacFarlane, J. J., & Cohen, D. H. 2001, ApJ, 554, L55
Chlebowski, T., Harnden, F. R., & Sciortino, S. 1989, ApJ, 341, 427
Cohen, D. H., Leutenegger, M. A., Grizzard, K. T., et al. 2006, MNRAS, 368,1905
Dere, K. P., Landi, E., Young, P. R., & Del Zanna, G. 2001, ApJS, 134, 331
Dessart, L., & Owocki, S. P. 2005, A&A, 437, 657
Ebbets, D. 1982, ApJS, 48, 399
Feldmeier, A., Oskinova, L., & Hamann, W.-R. 2003, A&A, 403, 217
Gabriel, A. H., & Jordan, C. 1969, MNRAS, 145, 241
Grevesse, N., & Sauval, A. J. 1998, in Solar Composition and its Evolution – From Core to Corona, ed. C. Frölich, M. C. E. Huber, S. K. Solanki, & R. von Steiger, Space Sci. Rev., 85, 161
Grevesse, N., & Sauval, A. J. 1999, A&A, 347, 348
Groenewegen, M. A. T., & Lamers, H. J. G. L. M. 1989, A&AS, 79, 359
Howk, J. C., Cassinelli, J. P., Bjorkman, J. E., & Lamers, H. J. G. L. M. 2000, ApJ, 534, 348
Ignace, R., & Gayley, K. G. 2002, ApJ, 568, 954
Kaastra, J. S., Mewe, R., & Nieuwenhuijzen, H. 1996a, in UV and X-ray Spectroscopy of Astrophysical and Laboratory Plasmas, ed. K. Yamashita, & T. Watanabe (Tokyo: Universal Academy Press, Inc.), 411 (SPEX)

Kaastra, J. S., Mewe, R., Liedahl, D. A., et al. 1996b, A&A, 314, 547
Kaper, L., Henrichs, H. F., Nichols, J. S., et al. 1996, A&AS, 116, 257
Kaper, L., Henrichs, H. F., Fullerton, A. W., et al. 1997, A&A, 327, 281
Kaper, L., Henrichs, H. F., Nichols, J. S., & Telting, J. H. 1999, A&A, 344, 231
Kitamoto, S., Tanaka, S., Suzuki, T., et al. 2000, Adv. Space Res., 25, 527
Kelly, R. L. 1987, J. Phys. Chem. Ref. Data, 16, Suppl. 1
Lamers, H. J. G. L. M., & Leitherer, C. 1993, ApJ, 412, 771
Lamers, H. J. G. L. M., Haser, S., de Koter, A., & Leitherer, C. 1999, ApJ, 516, 872
Lanz, T., & Hubeny, I. 2003, ApJS, 146, 417
Leutenegger, M. A., Paerels, F. B. S., Kahn, S. M., & Cohen, D. H. 2006, ApJ, 650, 1096
Leutenegger, M. A., Owocki, S. P., Kahn, S. M., & Paerels, F. B. S. 2007, ApJ, 659, 642
Lucy, L. B. 1982, ApJ, 255, 286
Lucy, L. B., & Solomon, P. M. 1970, ApJ, 159, 879
Mewe, R., Gronenschild, E. H. B. M., & van den Oord, G. H. J. 1985, A&AS, 62, 1 (MEKAL)
Mewe, R., Kaastra, J. S., & Liedahl, D. A. 1995, Legacy 6, 16 (MEKAL)
Miller, N. A. 2002, Understanding the High-Resolution X-Ray Spectra of Early-Type Stars, Ph.D. dissertation, University of Wisconsin, Madison, USA
Miller, N. A., Cassinelli, J. P., Waldron, W. L., MacFarlane, J. J., & Cohen, D. H. 2002, ApJ, 577, 951
Morrison, R., & McCammon, D. 1983, ApJ, 270, 119
Ness, J.-U., Mewe, R., Schmitt, J. H. M. M., et al. 2001, A&A, 367, 282
Oskinova, L. M., Feldmeier, A., & Hamann, W.-R. 2006, MNRAS, 372, 313
Owocki, S. P., & Cohen, D. H. 2006, ApJ, 648, 565
Owocki, S. P., Castor, J. I., & Rybicki, G. B. 1988, ApJ, 335, 914
Pollock, A. M. T. 2007a, A&A, 463, 1111
Pollock, A. M. T. 2007b, Status of the RGS Calibration, http://xmm.esac.esa.int/external/xmm_sw_cal/calib/documentation/index.shtml#RGS, 13
Porquet, D., Mewe, R., Dubau, J., Raassen, A. J. J., & Kaastra, J. S. 2001, A&A, 376, 1113
Snow, T. P. 1977, ApJ, 217, 760
Vacca, W. D., Garmany, C. D., & Shull, J. M. 1996, ApJ, 460, 914
Waldron, W. L., & Cassinelli, J. P. 2001, ApJ, 548, L45
Waldron, W. L., & Cassinelli, J. P. 2007, ApJ, accepted [arXiv:0707.0024]

Online Material

Appendix A:

References:
- Berghöfer, T. W., & Schmitt, J. H. M. M. 1994, A&A, 290, 435
- Berghöfer, T. W., Schmitt, J. H. M. M., & Cassinelli, J. P. 1996, A&AS, 118, 481 (Erratum: A&A 121, 212)
- Bisiacchi, G. F., López, J. A., & Firmani, C. 1982, A&A, 107, 252
- Blaauw, A. 1991, in: The Physics of Star Formation and Early Stellar Evolution, ed. C. J. Lada, & N. D. Kylafis, NATO ASI Ser. C, 342 (Dordrecht: Kluwer), 125
- Bohannan, B., & Garmany, C. D. 1978, ApJ, 223, 908
- Brown, A. G. A., de Geus, E. J., & de Zeeuw, P. T. 1994, A&A, 289, 101
- Chlebowski, T., Harnden, F. R., & Sciortino, S. 1989, ApJ, 341, 427
- ESA 1997, The Hipparcos Catalogue, ESA SP-1200
- Feldmeier, A., Puls, J., & Pauldrach, A. W. A. 1997, A&A, 322, 878
- Hanbury-Brown, R., Davis, J., & Allen, L. R. 1974, MNRAS, 167, 121
- Hummel, C. A., White, N. M., Elias, N. M., Hajian, A. R., & Nordgren, T. E. 2000, ApJ, 540, L91
- Kaper, L., Henrichs, H. F., Nichols, J. S., et al. 1996, A&AS, 116, 257
- Mason, B. D., Gies, D. R., Hartkopf, W. I., et al. 1998, AJ, 115, 821
- Penny, L. R. 1996, ApJ, 463, 737
- Voels, S. A., Bohannan, B., Abbott, D. C., & Hummer, D. G. 1989, ApJ, 340, 1073
- Walborn, N. R., & Fitzpatrick, E. L. 1990, PASP, 102, 379
- de Zeeuw, P. T., Hoogerwerf, R., de Bruijne, J. H. J., Brown, A. G. A., & Blaauw, A. 1999, AJ, 117, 354

Table A.1. Stellar parameters of ζ Ori.

Parameter	ζ Ori Aa	ref.	ζ Ori Ab	ref.	ζ Ori B	ref.	ζ Ori C	ref.
HR	1948				1949			
HD	37742				37743			
ADS	4263 A				4263 B		4263 C	
d (kpc)			$0.25^{+0.06\ a}_{-0.04}$					ESA97
E_{B-V} (mag)			0.06					VB89
A_V (mag)			0.19					
$\log N_{\rm H}$ (cm^2) (ISM)			20.34					FP97
separation (arcsec)			0.045	HW00	2.42	MG98	57.6	MG98
P (yr)					1509	MG98		
spectral type	O9.7 Ib	WF90	late O V	HW00	B2 III			
$\theta_{\rm D}$ (mas)	0.48 ± 0.04	HD74						
V (mag)	2.03	VB89	4	HW00	4.2	HW00	9	HW00
$B-V$ (mag)	-0.21	VB89						
$(B-V)_{\rm o}$ (mag)	-0.27	VB89						
$v_{\rm rad}$ (km s^{-1})	$+25 \pm 5$	BG78						
$v \sin i$ (km s^{-1})	123 ± 3	Pe96						
v_∞ (km s^{-1})	1885	KH96						
T_* (kK)	31.5 ± 1	FP97						
M (M$_\odot$)	34	VB89						
$\log g$ (cgs)	3.2 ± 0.1	VB89						
BC (mag)	-3.16	VB89						
$\log L/L_\odot$	5.2 [b]	FP97						
$\dot{M}$ (10^{-6} $M_\odot$ yr^{-1})	1.4 [b]	FP97						
$Y = n_{\rm He}/n_{\rm H}$	0.1	VB89						
$A_{\rm N}$	normal	BL82						
$T_{\rm x}^{\rm Einstein-ipc}$ (keV)	0.46 ± 0.08	CH89						
$\log L_{\rm x}^{\rm Einstein-ipc}$ (erg s^{-1})	32.1 ± 0.24 [b]	CH89						
$T_{\rm x}^{\rm ROSAT}$ (keV)	0.22	BS96						
$\log L_{\rm x}^{\rm Rosat}$ (erg s^{-1})	32.0 [b,c]	BS96						

Notes:

[a] The distance to ζ Ori is subject to debate. The three bright Belt stars in Orion, δ Ori (O9.5 II+B0.5 III), ϵ Ori (B0 Ia), and ζ Ori, form the high-luminosity end of the Ori OB1b subgroup, which has an estimated age between 7 Myr (Blaauw 1991) and 1.7 Myr (Brown et al. 1994). The distance to Ori OB1b had been estimated to be 360 ± 70 pc based on photometry (Brown et al. 1994), or 473 ± 33 pc based on *Hipparcos* parallax and proper motion measurements (de Zeeuw et al. 1999). We adopt here the direct *Hipparcos* parallax measurement of ζ Ori, corresponding to the distance as given above.

[b] Paramater scaled to $d = 0.25$ kpc.

[c] Berghöfer & Schmitt (1994) report that ζ Ori showed no evidence for variability over a three year time span, except for a two day period in September 23−25, 1992, when an increase of ∼15% in the X-ray count rate was measured.

References:

BG78: Bohannan & Garmany (1978); BL82: Bisiacchi et al. (1982); BS96: Berghöfer et al. (1996); CH89: Chlebowski et al. (1989); ESA97: ESA (1997); FP97: Feldmeier et al. (1997); HD74: Hanbury-Brown et al. (1974); HW00: Hummel et al. (2000); KH96: Kaper et al. (1996); MG98: Mason et al. (1998); Pe96: Penny (1996); VB89: Voels et al. (1989); WF90: Walborn & Fitzpatrick (1990).